RSC Advances

This is an *Accepted Manuscript*, which has been through the Royal Society of Chemistry peer review process and has been accepted for publication.

Accepted Manuscripts are published online shortly after acceptance, before technical editing, formatting and proof reading. Using this free service, authors can make their results available to the community, in citable form, before we publish the edited article. This *Accepted Manuscript* will be replaced by the edited, formatted and paginated article as soon as this is available.

You can find more information about *Accepted Manuscripts* in the **Information for Authors**.

Please note that technical editing may introduce minor changes to the text and/or graphics, which may alter content. The journal's standard **Terms & Conditions** and the **Ethical guidelines** still apply. In no event shall the Royal Society of Chemistry be held responsible for any errors or omissions in this *Accepted Manuscript* or any consequences arising from the use of any information it contains.

PVP-derived Carbon Nanofibers Harvesting Enhanced Anode Performance for Lithium Ion Batteries

Litian Dong[a], Guowen Wang[b], Xifei Li[a]*, Dongbin Xiong[a], Bo Yan[a], Baoxian Chen[a],

Dejun Li[a]*, Yanhua Cui[c]*

[a]Energy & Materials Engineering Centre, College of Physics and Materials Science, Tianjin Normal University, Tianjin 300387, China. E-mail: xfli2011@hotmail.com; dejunli@mail.tjnu.edu.cn

[b]Beijing Aerospace Propulsion Institute, Beijing 100076, China.

[c]Institute of Electronic Engineering, CAEP, Mianyang 621900, China. E-mail: cuiyanhua@netease.com

Abstract

The Co-embedded carbon nanofibers were synthesized using electrospinning with polyvinylpyrrolidone (PVP) instead of high cost polyacrylonitrile (PAN). The obtained composite nanofibers as an anode material for lithium ion batteries deliver a reversible capacity of 542.6 mAh g^{-1} in the 100th cycle at a current density of 100 mA g^{-1}. Moreover, the anode material shows better cycle performance and rate capability in comparison to the resultant product without Co additive. It is believed that the significant improvement is attributed to the nanofiber morphology with high surface-to-volume ratio as well as the existence of Co nanoparticles enhancing

1

electrical conductivity of the nanocomposites.

1. Introduction

In the last decades, rechargeable lithium ion batteries (LIBs) have been widely used in some applications of energy storage devices, such as cell phones, portable electronic devices and electrical vehicles. The carbon materials (i.e. graphite) have been successfully commercialized as anodes in LIBs.[1, 2] Besides the most pervasive graphite, some other carbon materials have been investigated including graphene,[3] carbon nanotubes,[4] porous carbons,[5] carbon nanofibers,[6, 7] etc. Among these materials, the carbon nanofibers have been attracted a lot of attention as one of the promising anode materials, owing to high surface-to-volume ratios, increased lithium ion transmission channel, and more lithium ions insertion sites on the electrode surface.[8-13] As a result, the carbon nanofibers exhibit improved reversible capacity and cycling stability than non-morphology carbon materials. For instance, the carbon nanofibers could show a reversible capacity of about 400 mAh g^{-1} after 40 cycles at a current of 50 mA g^{-1}.[14] By contrast, the specific capacities of non-morphology carbon materials drop down to 100~200 mAh g^{-1} after 100 cycles.[15] However, it still encounters a significant challenge to synthesize carbon nanofibers with low cost and high LIB performance.

Recently, an electrospinning technique[16-20] has received extensive attention to produce nanofibers through a simple, inexpensive and highly reproducible process.[21]

In the earliest stage, the carbon fibers were obtained using the viscose fiber for the space shuttle and the high-end field via electrospinning.[22] Then, polyacrylonitrile (PAN) as the precursors[23-26] was utilized to synthesize the carbon fibers. Subsequently, a series of polymers, such as asphalt, phenolic aldehyde, polyvinyl alcohol (PVA) etc,[23, 27] were applied to produce the carbon nanofibers. However, higher cost of the aforementioned precursors, as previously reported,[28] inevitably increased the carbon nanofiber price, which highly prevents them from further applications. By contrast, Poly(vinylpyrrolidone) (PVP) with lower cost and environmental friendly,[29, 30] has been a potential precursor to fabricate carbon nanofibers. Unfortunately, little research was reported to focus on PVP derived carbon nanofibers via electrospinning.

In this study, we synthesize the carbon nanofibers using the cheaper precursor of PVP via electrospinning. More importantly, some metal Co was successfully introduced into the carbon nanofibers. The Co nanoparticles as catalyst could create some graphitic carbon with high electrical conductivity. It is expected that the nanocomposites can increase anode cycling performance with the help of Co introduction into the carbon nanofibers. [31]

2. Experimental details

2.1 Synthesis of PVP-C and PVP-CNF

Poly(vinylpyrrolidone) (PVP, Aldrich, Mw=1,300,000g/mol) as precursors, and N,N-dimethyformatide (DMF) as the solvent were utilized to produce the carbon

nanofibers. Cobalt acetate tetrahydrate ($Co(CH_3COO)_2 \cdot 4H_2O$) was used as the source

of Co. A typical process is as follows. Firstly, 1.5g PVP was dissolved into the mixed

solution of 5mL of acetate and 5mL of DMF for 3h under magnetic stirring. Secondly,

0.5g cobalt acetate tetrahydrate ($Co(CH_3COO)_2 \cdot 4H_2O$) was dissolved in 5mL of

deionized water for 1h. Then, two solutions were mixed for 2h. The mixture was

transferred to a plastic injector, and electrospun on a pink film on a clean wiper

wrapped around a cylinder collector at a rotation speed of 0.03 mm min^{-1}, at a DC

voltage of 20kV with a flow rate of 0.18 mL h^{-1}. The distance between the collector

and the needle was kept at 10 cm. Finally, as-collected precursor fibers were dried in

air at 80 ^{o}C overnight. The resultant materials were annealed at 300 ^{o}C for 3h, and

next rose to 500 ^{o}C for 3h in Ar atmosphere. The Co-embedded carbon nanofibers

were produced, which was marked as PVP-CNF. For comparison, the pristine carbon,

marked as PVP-C, was obtained by the similar method without introduction of

$Co(CH_3COO)_2 \cdot 4H_2O$. In addition, PAN was employed as carbon source to synthesize

carbon nanofiber (PAN-CNF) using similar electrospinning parameter.

2.2 structural characterizations

Surface morphologies of the materials were observed via a scanning electron

microscope (SEM, SU8010, Hitachi Jaoan) equipped with energy dispersive X-ray

(EDX, INCAx-sight, Oxford). The phase and crystallinity of the carbon nanofibers

was studied on a powder X-ray diffraction (XRD), which were recorded on X-ray

diffractometer (DX-2700) with Cu K$_{\alpha}$ radiation. High resolution images of

microstructures and selected area electron diffraction (SAED, JEOL JEM-3000F) patterns were obtained with a transmission electron microscope (TEM, JEOJ JEM-3000F). Thermal properties were tested by a thermal gravimetric analyzer (TGA, Pyris Diamond6000 TG/DTA, PerkinElmer Co, America) in air over a temperature range of room temperature to 800 $^{\circ}$C at a heating rate of 10 $^{\circ}$C min^{-1}. Raman spectra were recorded through Jobin-Yvon Horiba HR800.

2.3 electrochemical measurements

The working electrode was prepared by casting a homogeneous slurry consisting of the active materials, conductive carbon black, polyvinylidone difluoride (PVDF) (the weight ratio of 80:10:10) in N-methyl-2-pyrrolidone(NMP) on the copper foil. Then the electrodes were dried under vacuum at 100°C for overnight. The electrodes were cut in 12 mm diameter disks. The electrolyte was 1 M LiPF$_6$ dissolved in a mixture of ethylene carbonate (EC) and diemethyl carbonate (DMC) in a ratio of 1:1 by volume. The CR2032-type coin cells were assembled in an argon-filled glovebox. Galvanostatic charge-discharge cycles were performed using a Land battery test system (LANHE CT2001A) in the voltage of 0.01-3V at room temperature. Electrochemical impedance spectroscopy (EIS) was recorded between 200 kHz and 5 mHz with an amplitude of 5 mV on a VMP3 (Princeton Applied Research).

3. Results and Discussion

Scheme 1. shows the formation procedures of the PVP-CNF: (i) to form the smooth

nanofibers using the precursor solution of $Co(CH_3COO)_2\cdot 4H_2O$ and PVP via

electrospinning. (ii) to obtain the PVP-CNF by annealing in Ar atmosphere. The

carbon content of the PVP-CNF is confirmed by TGA, as shown in Fig.1a. A sharp

weight variety occurs at about $390^{\circ}C$, indicating the oxidation of carbon with the

weight loss. It is worth to note that the oxidation of Co in air can trigger the weight

raise. As shown the Fig.1a, the content of the Co_3O_4 in the sample is 38.35%. The Co

content in the composites is based on the equation $3W_{Co}\times X_{Co3O4}/W_{Co3O4}= X_{Co}$, where

W_{Co} and W_{Co3O4} are relative molecular mass of Co and Co_3O_4, respectively. X_{Co3O4} is

the residual weight percentage, and X_{Co} is the Co content in the composites. The

calculated result of X_{Co} is 28.17 wt%, thus, the content of carbon nanofibers in the

composites is 71.83 wt%. In addition, the decomposition temperature of the two

materials are different (see Fig. 1a), which illustrates that the existed Co grains result

in lower decomposition temperature. Fig. 1b represents the EDX results of the PVP-C

and PVP-CNF. The PVP-C consists of the C and O element. In addition of C and O,

Co element was observed in the Co-carbon nanofibers. In the Raman spectra of the

PVP-CNF (Fig. 1c), two main peaks are situated at 1350 and 1580 cm^{-1}, which are

designated as the D band and G band, respectively. The G band is associated with

graphitic carbon, while the D band is attributed to amorphous carbon. In addition, the

relative intensity of D band against G band (I_D/I_G) represents the degree of disorder in

the graphite structure. The Raman spectrum of the PVP-CNF shows the ratio of the

I_D/I_G is ~ 0.82, which further confirms the existence of graphitic carbon. It is worth

6

nothing that the PVP-C suffered from the fluorescence reaction, as a result, Raman signal of PVP-C is not obvious (see the inset of Fig. 1c). Fig. 1d displays XRD patterns of the PVP-C and the PVP-CNF. The main peaks of PVP-CNF can be observed at 2θ of about 44.2^o, 51.5^o, 75.9^o, corresponding to (111), (200) and (220) lattice planes of Co, respectively. And the broad peak ($2\theta=26°$) of the PVP-C corresponds to the (002) plane of carbon material.

Fig. 2 shows the SEM images of the PVP-C and PVP-CNF. Before carbonization, both samples display similar smooth nanowired morphologies in diameters with the range of 400-500nm (see Fig. 3a and 3b). After thermal treatment, the nanofibers in Fig. 2a totally disappear, as shown in Fig. 2c. More interestingly, the Co-contained sample still keeps nanowired structure (Fig. 2d) with decreased diameters. It can be also observed that a lot of Co nanograins are uniformly deposited along the nanofibers. The SEM images of PAN-CNF before and after carbonization are shown in the Fig. 2e and 2f. As expected, the carbon nanofibers can be obtained when the PAN is used as the carbon source via electrospinning, which differs from the product of PVP in Fig. 2c. By contrast, the diameter of PVP-CNF is obviously smaller than that of PAN-CNF. The elemental mappings in Fig. 2g and 2h prove that the Co nanograins are evenly distributed along the carbon nanofibers. It is worth mentioning that after carbonization, the Co-carbon nanofibers can still maintain the morphology of the nanofibers originating from the existence of the Co nanograins. Furthermore, further examination in high resolution TEM has revealed that the Co nanograins are evenly distributed in the carbon nanofibers. The size of the Co nanograins is about 10 nm. In addition, as

apparent from Fig. 3b, some graphitic carbon is formed around the Co nanograins. It proves that the Co nanograins function as the catalyst, and facilitate the increase of graphitization.

Fig. 4a compares the cycling performance of PVP-CNF, Co_3O_4 nanofibers and PVP-C at the current density of 100 mA g^{-1} at the voltage range of 0.01V to 3V. Clearly, three samples exhibit various cycling performance. Both Co_3O_4 nanofibers and PVP-C deliver poor performance. By contrast, the PVP-CNF material shows better cyclical stability and higher reversible capacity. As expected, the introduction of Co in the nanocomposites significantly enhances anode performance. For instance, in the 100th cycle, the reversible capacities of the PVP-C, Co_3O_4 nanofibers and PVP-CNF are 449.8, 430.5 and 766 mAh g^{-1}, respectively. The PVP-CNF and PVP-C are examined at various current densities of 50, 100, 150, 200, and 250 mA g^{-1}. As shown in Fig. 4b, the PVP-CNF possesses better rate capability and higher capacity retention as compared with PVP-C. It was reported that the suppression of the formation of SEI on the active material by Co nanograins is another pivotal factor to enhance the rate capabilities.[32] At each current density, the average discharge capacities of PVP-CNF are 821.8, 707.6, 677.6, 660.2, 650.5 mAh g^{-1}, respectively, which are much higher than those of PVP-C (549.7, 476.3, 455.3, 443.7, 435 mAh g^{-1}).

Fig. 4c and 4d show charge-discharge behaviors of the PVP-C and the PVP-CNF electrodes in the 1st, $2^{nd,}$ 5th 10th 20th and 50th cycles over a voltage ranging from 0.01 to 3.0V at a current density of 100 mA g^{-1}. The initial discharge and charge capacities

of the PVP-C are 1338.7 and 670.2 mAh g^{-1}, respectively. By contrast, the PVP-CNF reveals higher initial discharge and charge capacities of 1770.7 and 1025.7 mAh g^{-1}, respectively. The reason causing the initial irreversible capacity is some side reactions such as the formation of solid electrolyte interface (SEI) film. The PVP-CNF anode exhibits high reversible capacity of about 932.3 mAh g^{-1} at the second cycle with a 95.6% coulombic efficiency. After 50 cycles, the coulombic efficiency of PVP-CNF increases to 98.3%, and the capacity drops down to about 639.9 mAh g^{-1}, which corresponds to 68.6% of capacity retention in comparison to that of the second cycle. The average capacity fade rates of PVP-CNF and PVP-C are 0.18% and 0.33% per cycle during 100 cycles. It indicated that the reversible capacity and capacity retention of PVP-CNF are higher than that of the PVP-C, which is attributed to the unique nanostructure of PVP-CNF. The effects of the nanofiber structures and Co nanograins on electrochemical performance are as-following: (i) to enhance charge transfer and electron conduction, and decrease inner resistance. (ii) more surface area is available for Li ion diffusion and shortens the Li ion diffusion path way.

As shown in the inset of Fig. 4c and 4d, electrochemical polarization can be observed during rest period of testing cells. The polarization voltage is defined as the difference between the 3V and the voltage onset. The relationship between the polarization voltage and cycle number is shown in the Fig. 4e. As can be seen, the polarization voltage of PVP-C is larger than that of PVP-CNF. The result indicates that the incorporation of Co nanograins within the PVP-CNF can significantly decrease the resistance polarization. Furthermore, to further confirm the improved

electrochemical reaction kinetics of PVP-CNF electrode, EIS of PVP-C and PVP-CNF after 5 cycles were carried out within the frequency range of 100 kHz to 10 mHz, and the Nyquist plots were shown in Fig. 4f. To obtain kinetics parameters, we employed the two RC parallel circuits to simulate the impedance spectra on the basis of the potential SEI layer. In the equivalent circuit (inset of Figure 4f), R_s represents the ohmic resistance of whole reaction system, and R_{sf} is the resistance of the SEI film. R_{ct} is the charge transfer resistance related to the electrochemical reaction. Constant phase element (CPE) was employed in the equivalent circuits instead of pure capacitance owing to the inhomogeneous surface of the working electrode. CPE_{sf} and CPE_{ct} are constant phase elements corresponding to the surface film and double-layer capacitance, respectively. W_{dif} stands for Warburg impedance associated with solid state diffusion.[33] Based on the equivalent circuits, the obtained kinetics parameters are listed in Table 1. One can observe that the R_s value of PVP-CNF is 11.3Ω, which is lower than that of PVP-C (17.1Ω). This result is consistent with the resistance polarization presented in Fig. 4e. Moreover, it is seen that the R_{sf} of PVP-CNF is lower, which can be due that the Co nanograins may restrain the formation of the SEI film. PVP-CNF shows the lower R_{ct} as compared with the PVP-C, which is attributed to the improved electrical conductivity of PVP-CNF.[34, 35] These results indicate that the ohmic resistance of whole reaction system and the charge-transfer resistance of PVP-CNF anode are smaller than those of the PVP-C, and further illustrate the fact that electrochemical reaction kinetics of PVP-CNF electrode is improved, which might be one of the key factors contributing to enhanced electrochemical performance

of the PVP-CNF.

4. Conclusions

In summary, PVP-CNF was reasonably designed and successfully synthesized using a simple and environmentally benign electrospinning method. Compared with PVP-C, PVP-CNF is proved to be a promising anode, showing higher reversible capacity, superior cycling durability, increasing rate capability. It can be ascribed to both the existence of Co nanograins leading to the formation of the carbon nanofibers with the high specific surface area, and the Co nanograins embedded in the carbon fibers which increase the electrical conductivity. The existence of the Co nanograins can result in the formation of the carbon nanofibers. The nanofibered composites effectively enhance electrical conductivity of electrode and thereby increase cycling performance of the anode materials. Therefore, this work will open an opportunity to create high performance carbon nanofibers as electrodes for lithium-ion batteries.

Acknowledgments

References

1.   W. Zhang and P. N. Pintauro, *ChemSusChem*, 2011, **4**, 1753-1757.

2.   J. Li, C. Daniel and D. Wood, *Journal of Power Sources*, 2011, **196**, 2452-2460.

3.   G. Wang, X. Shen, J. Yao and J. Park, *Carbon*, 2009, **47**, 2049-2053.

4.   J. J. Gooding, *Electrochimica Acta*, 2005, **50**, 3049-3060.

5.   K.-S. Kim and S.-J. Park, *Journal of Power Sources*, 2013, **244**, 792-798.

6.   I. Rajzer, R. Kwiatkowski, W. Piekarczyk, W. Biniaś and J. Janicki, *Materials Science and Engineering: C*, 2012, **32**, 2562-2569.

7.   X. Su, Q. Wu, X. Zhan, J. Wu, S. Wei and Z. Guo, *J Mater Sci*, 2012, **47**, 2519-2534.

8.   Y. Yu, L. Gu, C. Wang, A. Dhanabalan, P. A. van Aken and J. Maier, *Angewandte Chemie International Edition*, 2009, **48**, 6485-6489.

9.   I. Meschini, F. Nobili, M. Mancini, R. Marassi, R. Tossici, A. Savoini, M. L. Focarete and F. Croce, *Journal of Power Sources*, 2013, **226**, 241-248.

10.   Y.-H. Liu, T. Takasaki, K. Nishimura, M. Yanagida and T. Sakai, *Journal of Power Sources*, 2015, **290**, 153-158.

11.   R. Elazari, G. Salitra, A. Garsuch, A. Panchenko and D. Aurbach, *Advanced*

Materials, 2011, **23**, 5641-+.

12. Y. Zhang and A. L. Yarin, *Langmuir : the ACS journal of surfaces and colloids*, 2011, **27**, 14627-14631.

13. M. H. Kjell, E. Jacques, D. Zenkert, M. Behm and G. Lindbergh, *J. Electrochem. Soc.*, 2011, **158**, A1455-A1460.

14. J. Yue, X. Zhao and D. Xia, *Electrochemistry Communications*, 2012, **18**, 44-47.

15. L. Jabbour, M. Destro, D. Chaussy, C. Gerbaldi, S. Bodoardo, N. Penazzi and D. Beneventi, *Composites Science and Technology*, 2013, **87**, 232-239.

16. J. W. Min, A. K. Kalathil, C. J. Yim and W. B. Im, *Materials Characterization*, 2014, **92**, 118-126.

17. F. L. Zhu, J. X. Zhao, Y. L. Cheng, H. B. Li and X. B. Yan, *Acta Phys.-Chim. Sin.*, 2012, **28**, 2874-2878.

18. X. Zhang, B. L. Shi and Y. Wang, *J. Adhes. Sci. Technol.*, 2012, **26**, 353-360.

19. I. Uslu, T. Tunc, M. K. Ozturk and A. Aytimur, *Polym.-Plast. Technol. Eng.*, 2012, **51**, 257-262.

20. G. Zhu, L. K. Pan, J. Yang, X. J. Liu, H. C. Sun and Z. Sun, *Journal of Materials Chemistry*, 2012, **22**, 24326-24329.

21. J. Wu, D. Zeng, X. Wang, L. Zeng, Q. Huang, G. Tang and C. Xie, *Langmuir : the ACS journal of surfaces and colloids*, 2014, **30**, 11183-11189.

22. E. Jacques, M. H. Kjell, D. Zenkert, G. Lindbergh, M. Behm and M. Willgert, *Composites Science and Technology*, 2012, **72**, 792-798.

23. C. W. Cho, D. Cho, O. H. Kwon, Y.-G. Ko and I.-K. Kang, *Carbon Letters*, 2007, **8**, 313-320.

24. G. Y. Oh, Y. W. Ju, H. R. Jung and W. J. Lee, *J. Anal. Appl. Pyrolysis*, 2008, **81**, 211-217.

25. S. A. H. Ravandi and M. Sadrjahani, *J. Appl. Polym. Sci.*, 2012, **124**, 3529-3537.

26. K. Nasouri, H. Bahrambeygi, A. Rabbi, A. M. Shoushtari and A. Kaflou, *J. Appl. Polym. Sci.*, 2012, **126**, 127-135.

27. P. Lian, J. Wang, D. Cai, L. Ding, Q. Jia and H. Wang, *Electrochimica Acta*, 2014, **116**, 103-110.

28. Y.-H. Liu, T. Takasaki, K. Nishimura, M. Yanagida and T. Sakai, *Journal of Power Sources*, 2015, **290**, 153-158.

29. T. L. Yang, C. T. Pan, Y. C. Chen, L. W. Lin, I. C. Wu, K. H. Hung, Y. R. Lin, H. L. Huang, C. F. Liu, S. W. Mao and S. W. Kuo, *Optical Materials*, 2015, **39**, 118-124.

30. M. Enculescu, A. Evanghelidis and I. Enculescu, *Journal of Physics and Chemistry of Solids*, 2014, **75**, 1365-1371.

31. X. Yu, Y. Fu, X. Cai, H. Kafafy, H. Wu, M. Peng, S. Hou, Z. Lv, S. Ye and D. Zou, *Nano Energy*, 2013, **2**, 1242-1248.

32. J. Liu and A. Manthiram, *Chemistry of Materials*, 2009, **21**, 1695-1707.

33. B. Yan, M. Li, X. Li, Z. Bai, L. Dong and D. Li, *Electrochimica Acta*, 2015, **164**, 55-61.

14

34.   R. Song, H. Song, J. Zhou, X. Chen, B. Wu and H. Y. Yang, *Journal of*

        Materials Chemistry, 2012, **22**, 12369-12374.

35.   F. G. Emmerich, *Carbon*, 1995, **33**, 1709-1715.
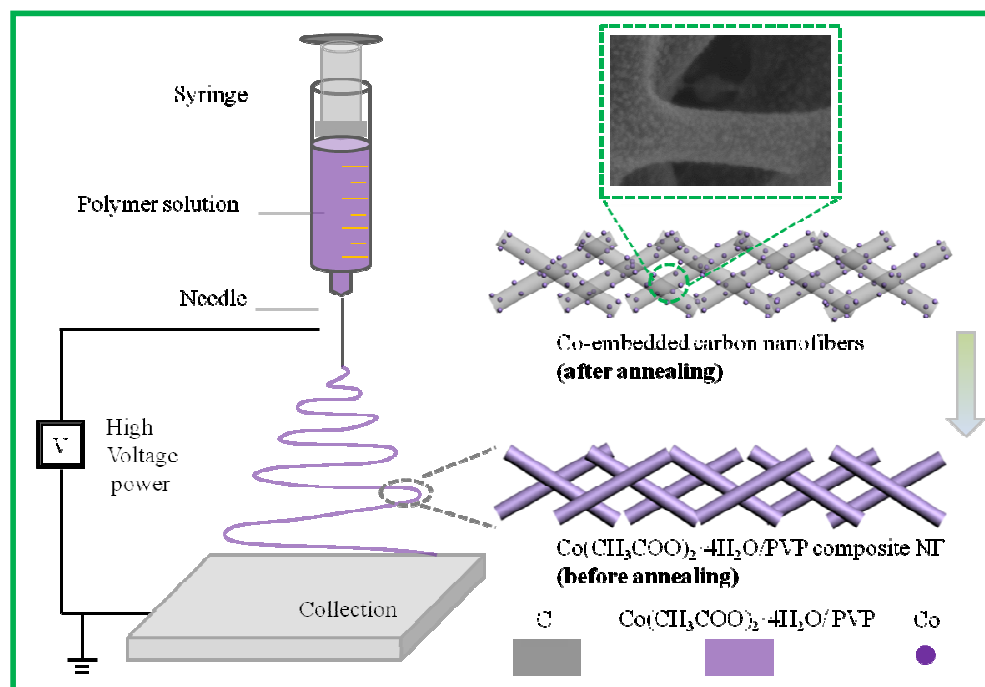
Scheme 1. Schematic illustration on the formation mechanism of PVP-CNF.
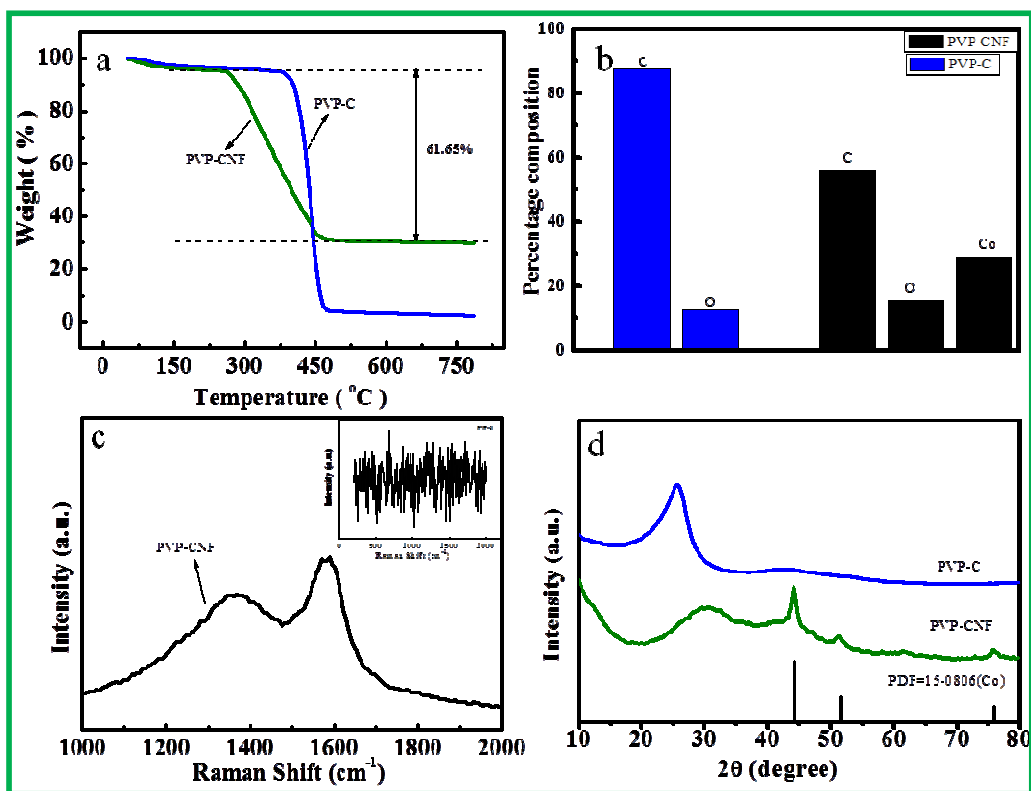
Fig. 1. (a) The TGA curves and (b) the EDX results of PVP-C and PVP-CNF; (c)

Raman spectra of PVP-CNF (the inset for PVP-C); (d) XRD patterns of PVP-C and

PVP-CNF.
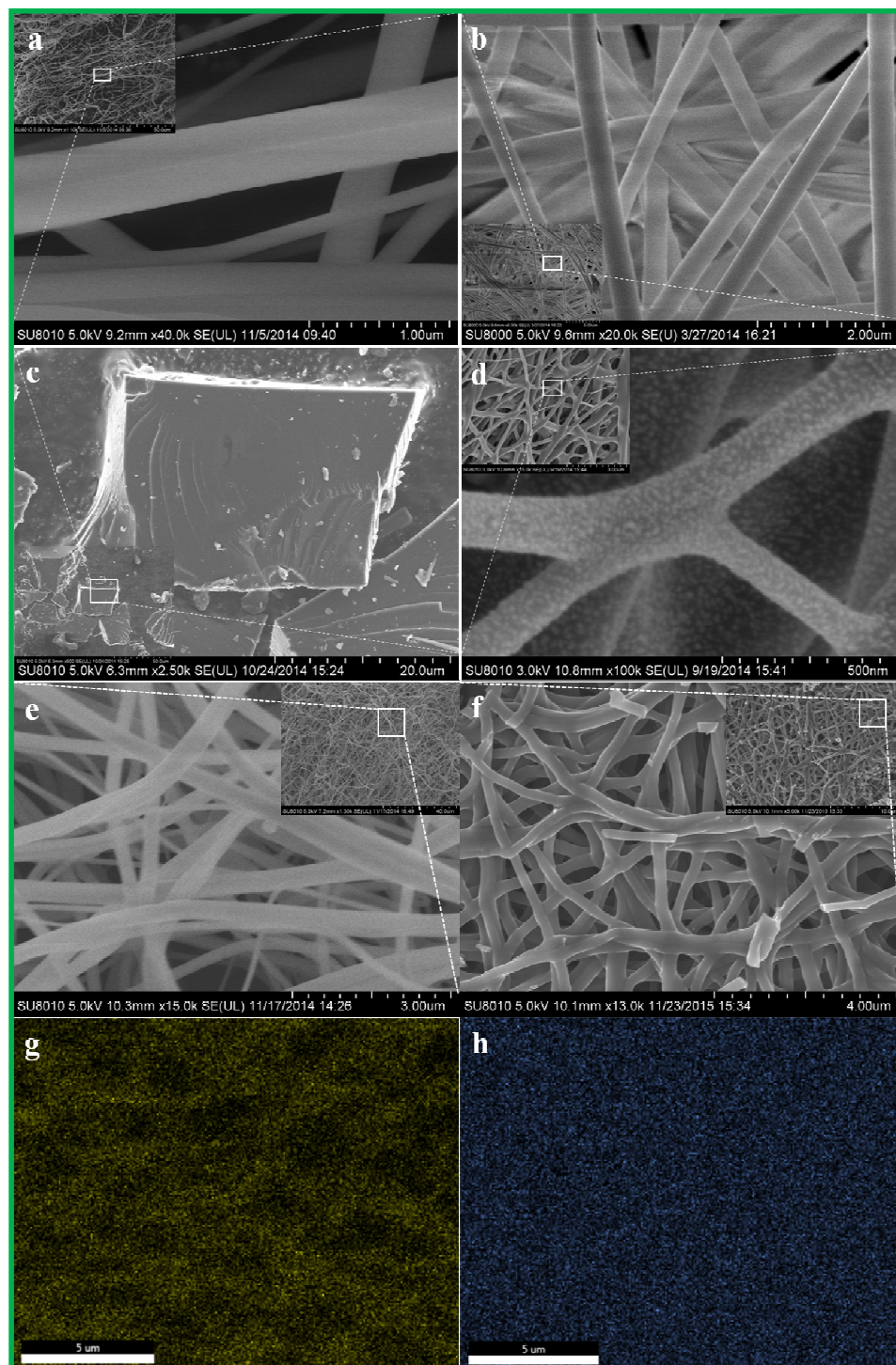
Fig. 2. SEM images of (a) PVP-C and (b) PVP-CNF before carbonization , (c) PVP-C

and (d) PVP-CNF PVP-C as well as (e) and (f) PAN-CNF before and after

carbonization; Elemental mapping analysis of (g) C element and (h) Co element in

PVP-CNF.
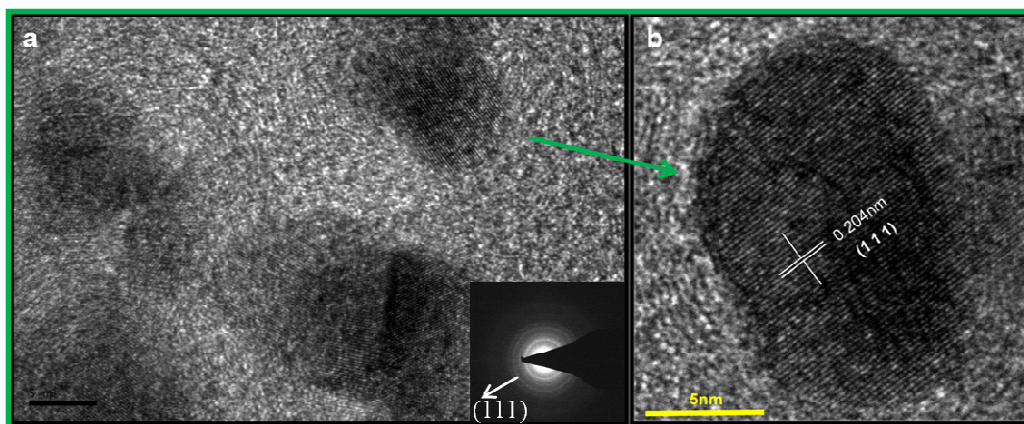
Fig. 3. TEM images of PVP-CNF at (a) low and (b) high magnification (the inset is

the selected area electron diffraction).
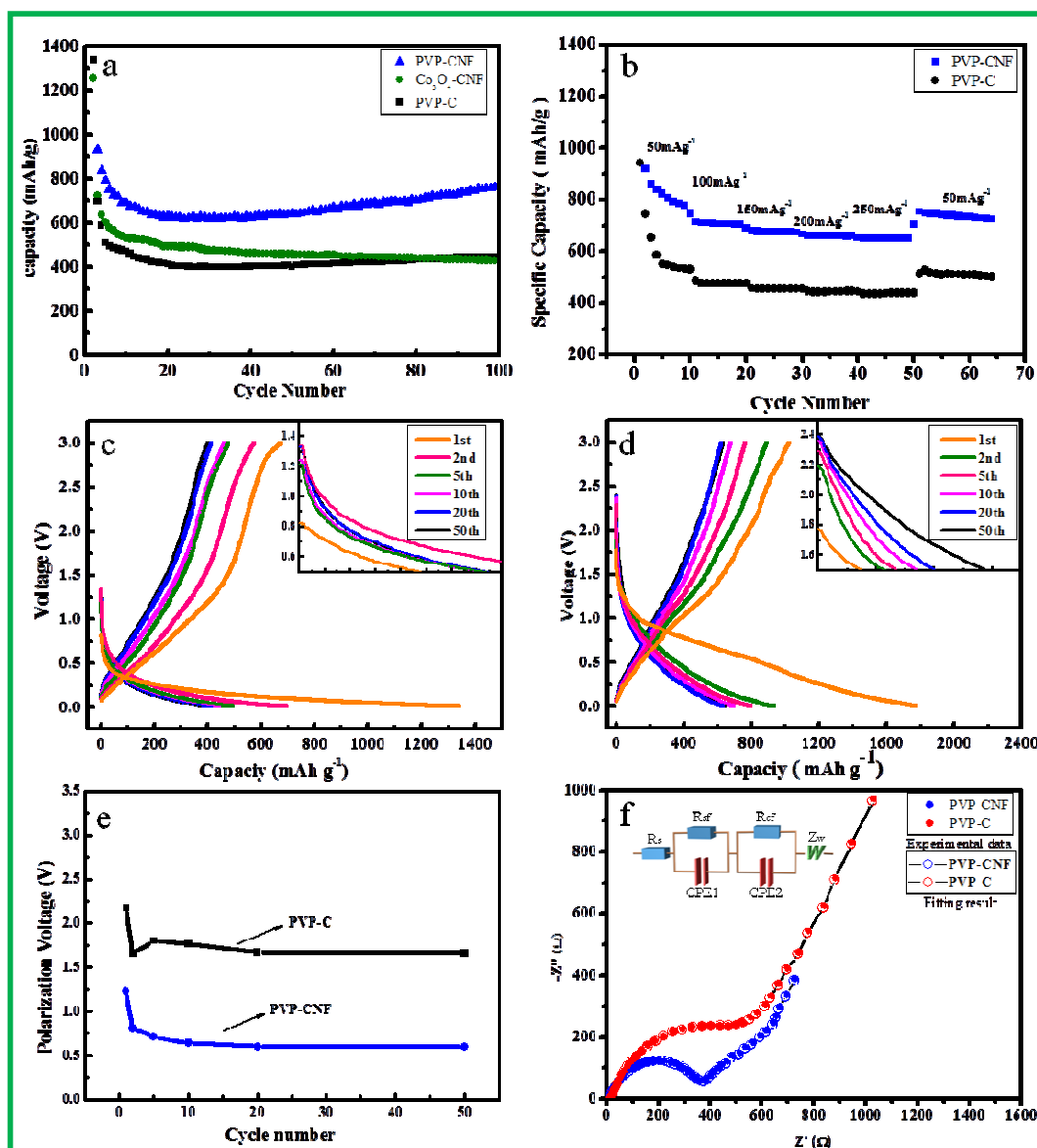
Fig. 4. (a) Cycling performance of the PVP-CNF, Co_3O_4-CNF and PVP-C; (b) Rate capability of PVP-CNF and PVP-C; The charge-discharge profiles of (c) PVP-C and (d) PVP-CNF, (e) Electrochemical polarization of the PVP-C and PVP-CNF; and (f) The EIS of PVP-C and PVP-CNF after cycling (the inset is the equivalent circuit).

Table 1. Kinetic parameters of PVP-CNF and PVP-C after 5 cycles

Sample	$R_s(\Omega)$	$R_{sf}(\Omega)$	$R_{ct}(\Omega)$
PVP-CNF	11.3	355.0	325.6
PVP-C	17.1	417.5	569.8

Graphical Abstract